Original Article

MOLECULAR METABOLISM

Genetic deletion of *Bco2* and *Isx* establishes a golden mouse model for carotenoid research

Linda D. Thomas, Srinivasagan Ramkumar, Marcin Golczak, Johannes von Lintig*

ABSTRACT

Objective: Low plasma levels of carotenoids are associated with mortality and chronic disease states. Genetic studies in animals revealed that the tissue accumulation of these dietary pigments is associated with the genes encoding β-carotene oxygenase 2 (BCO2) and the scavenger receptor class B type 1 (SR-B1). Here we examined in mice how BCO2 and SR-B1 affect the metabolism of the model carotenoid zeaxanthin that serves as a macular pigment in the human retina.

Methods: We used mice with a *lacZ* reporter gene knock-in to determine *Bco2* expression patterns in the small intestine. By genetic dissection, we studied the contribution of BCO2 and SR-B1 to zeaxanthin uptake homeostasis and tissue accumulation under different supply conditions (50 mg/kg and 250 mg/kg). We determined the metabolic profiles of zeaxanthin and its metabolites in different tissues by LC-MS using standard and chiral columns. An albino $Isx^{-/-}/Bco2^{-/-}$ mouse homozygous for Tyr^{c-2J} was generated to study the effect of light on ocular zeaxanthin metabolites.

Results: We demonstrate that BCO2 is highly expressed in enterocytes of the small intestine. Genetic deletion of *Bco2* led to enhanced accumulation of zeaxanthin, indicating that the enzyme serves as a gatekeeper of zeaxanthin bioavailability. Relaxing the regulation of SR-B1 expression in enterocytes by genetic deletion of the transcription factor ISX further enhanced zeaxanthin accumulation in tissues. We observed that the absorption of zeaxanthin was dose-dependent and identified the jejunum as the major zeaxanthin-absorbing intestinal region. We further showed that zeaxanthin underwent oxidation to ε,ε-3,3′-carotene-dione in mouse tissues. We detected all three enantiomers of the zeaxanthin oxidation product whereas the parent zeaxanthin only existed as (3R, 3′R)-enantiomer in the diet. The ratio of oxidized to parent zeaxanthin varied between tissues and was dependent on the supplementation dose. We further showed in an albino $Isx^{-/-}/Bco2^{-/-}$ mouse that supra-physiological supplementation doses (250 mg/kg) with zeaxanthin rapidly induced hypercarotenemia with a golden skin phenotype and that light stress increased the concentration of oxidized zeaxanthin in the eyes.

Conclusions: We established the biochemical basis of zeaxanthin metabolism in mice and showed that tissue factors and abiotic stress affect the metabolism and homeostasis of this dietary lipid.

Keywords BCO2; SR-B1; Carotenoid metabolism; Zeaxanthin; Absorption; Oxidation

1. INTRODUCTION

Carotenoids affect a rich variety of physiological functions in nature and are beneficial for human health serving as antioxidants in lipophilic environments and light filters in the skin [1]. The carotenoids, zeaxanthin and lutein, accumulate in high concentrations in the fovea centralis within the macula lutea of primate eyes [2,3]. The macular pigments filter short-wavelength light, decrease chromatic aberration, and prevent light damage to the photoreceptors [4,5]. Additionally, carotenoids such as β-carotene are the major precursors for retinoids (vitamin A and its derivatives) in the human diet [6]. Retinoids play vital roles as precursors for chromophores in vision and hormone-like compounds in a variety of physiological processes throughout the mammalian life cycle [7].

Low carotenoid status has been associated with a number of chronic disease states, including cardiovascular disease, cognitive impairments, and age-related macular degeneration (AMD) [5,8–10]. Studies indicating that zeaxanthin and lutein can reduce the progression of AMD have attracted broad clinical interest [11]. However, intervention trials revealed variable outcomes of the preventive effects of carotenoids on the incidence of chronic disease [8]. Indeed, long-term supraphysiological dosing of β-carotene has even proven to be

Department of Pharmacology, School of Medicine, Case Western Reserve University, Cleveland, OH, 44106, USA

*Corresponding author. Department of Pharmacology (W341), School of Medicine, Case Western Reserve University, 10900 Euclid Avenue, Cleveland, OH, 44106, USA. E-mail: johannes.vonlintig@case.edu (J. von Lintig).

Abbreviations: AMD, age-related macular degeneration; BCO2, β-carotene oxygenase 2; BDHL1, 3-hydroxybutyrate dehydrogenase 1-like; CCDs, carotenoid cleavage dioxygenases; ERG, electroretinography; eWAT, epididymal white adipose tissue; GRAMD1, gram-domain containing proteins; HPLC, high-pressure liquid chromatography; ISX, intestine specific homeobox; PFA, paraformaldehyde; OCT, optical coherence tomography; SR-B1, scavenger receptor class B type 1; TLC, thin-layer chromatography

Received May 3, 2023 • Revision received May 16, 2023 • Accepted May 19, 2023 • Available online 22 May 2023

https://doi.org/10.1016/j.molmet.2023.101742

harmful in some cases to people at risk of disease [12,13]. These findings suggest the existence of a therapeutic window for dietary carotenoids that is influenced by genetics and lifestyle [14].

Many vertebrates, including humans, absorb carotenoids intact and accumulate them in specific patterns in tissues [15]. However, mice the most common model for biomedical research do not accumulate the pigments in significant amounts. In the past decades, genes encoding proteins of carotenoid metabolism have been identified, including the gene encoding β-carotene-oxygenase 2 (BCO2) and the class B scavenger receptor type 1 (SR-B1) [16–19]. Mutations in the *BCO2* gene were established as important genetic factors that determine carotenoid tissue accumulation in vertebrates. *BCO2* mutations are associated with the yellow fat phenotype in bovine, sheep, and rabbits [20–22] and a yellow skin phenotype in chicken [23]. The *BCO2* gene encodes a carotenoid cleaving dioxygenase (CCD) that catalyzes oxidative cleavage at positions C9, C10 and C9′, C10' of the carbon backbone of many carotenoids and apocarotenoids [24,25]. The broad substrate specificity and the phenotype of BCO2 mutant animals indicate that BCO2 is the major carotenoid metabolizing enzyme. While mutations in the *BCO2* gene are associated with carotenoid excess, mutations in the gene encoding SR-B1 are associated with carotenoid deficiency [26]. Moreover, genetic polymorphism in the gene affects macula pigment density in the human eyes and was implicated as a genetic factor modulating AMD susceptibility [27,28].

Here, we studied the interplay of SR-B1 and BCO2 in the metabolism and homeostasis of the model carotenoid zeaxanthin in mice. We observed that BCO2 expression in enterocytes of the intestine serves as the gatekeeper for zeaxanthin absorption and body distribution. We further identified the transcription factor ISX as an important modulator of the intestinal activity of SR-B1 and zeaxanthin absorption. Zeaxanthin absorption was concentration-dependent and the parent compound underwent oxidation into ε,ε-3, 3′-carotene-dione enantiomers. We established an albino *Isx*$^{-/-}$/*Bco2*$^{-/-}$ mouse as a resourceful animal model to study carotenoid metabolism and to characterize the physiological roles and benefits of the pigments in a mammalian model. Similar to humans, this mouse model accumulates carotenoids and displays the pigments in the skin and eyes.

2. MATERIALS AND METHODS

2.1. Materials

All chemicals, unless otherwise stated, were purchased from Fisher Scientific and Sigma Aldrich. TRIzol RNA isolation reagent was obtained from Invitrogen. The anti-mouse and anti-rabbit horseradish peroxidase-conjugated secondary antibodies were purchased from Abcam (Cambridge, United Kingdom). RIPA buffer was purchased from Cell Signaling Technology (Danvers, MA). 3R,3′R-zeaxanthin beadlets were a gift from DSM (Sisseln, Switzerland).

2.2. Animals, husbandry, and experimental diets

All mice experiments in these studies were conducted using protocols approved by Case Western Reserve University's Institutional Animal Care and Use Committee (IACUC) and adhered to the guidelines of the Association for Research in Vision and Ophthalmology Statement for the Use of Animals in Ophthalmic and Vision Research. Both male and female mice on a pigmented C57BL/6 J or albino B6(Cg)-Tyrc-2J/J genetic background were used for this study. Wild-type (WT) mice were purchased from the Jackson laboratory. The generation of *Bco2*$^{-/-}$ mice in the C57BL/6 J background was previously described [29,30]. The generation of *Isx*$^{-/-}$/*Bco2*$^{-/-}$ mice on an albino B6(Cg)-Tyrc-2J/J background was carried out by conventional breeding between pigmented C57BL/6 J *Isx*$^{-/-}$/*Bco2*$^{-/-}$ and albino B6(Cg)-Tyrc-2J/J WT mice to generate B6(Cg)-Tyrc-2J/J *Isx*$^{-/-}$/*Bco2*$^{-/-}$ knockout mice. All mice were bred on a standard chow diet consisting of 15,000 IU vitamin A/kg (Prolab RMH 3000, LabDiet, St. Louis, MO, USA) at a vivarium located at Case Western Reserve University. Mice were raised on a dark/light cycle to maintain a circadian rhythm. The dark-raised mice were transferred immediately after weaning in a dark room for four weeks. At the end of the experimental period, mice were anesthetized using a drug cocktail of ketamine (20 mg/mL) and xylazine (1.7 mg/mL). Blood was drawn directly from the heart by cardiac puncture under deep anesthesia. Immediately after, mice were perfused with 20 mL of PBS and sacrificed by cervical dislocation for further tissue collection. The duodenum, jejunum, ileum, liver, kidney, eyes, and epididymal white adipose tissue (eWAT) were immediately harvested for analysis or snap frozen in liquid nitrogen and stored at −80 °C until further use.

2.3. Zeaxanthin dietary supplementation

After weaning (4 weeks old), male and female *Bco2*$^{-/-}$ and *Isx*$^{-/-}$/*Bco2*$^{-/-}$ mice were fed with a control diet without 3R,3′R-zeaxanthin (0 mg/kg 3R,3′R-zeaxanthin), 50 mg/kg 3R,3′R-zeaxanthin, or 250 mg/kg 3R,3′R-zeaxanthin for 4 weeks. Enantiomerically pure 3R,3′R-zeaxanthin, confirmed by chiral HPLC analysis, was used for dietary supplementation. Additionally, a cohort of WT mice was supplemented with 250 mg/kg 3R,3′R-zeaxanthin for 4 weeks. Both control and 3R,3′R-zeaxanthin diets were devoid of vitamin A. Diets containing 3R, 3′R-zeaxanthin were prepared by Research Diets (New Brunswick, NJ, USA) by incorporating a water-soluble formation of 3R,3'R-zeaxanthin beadlets (DSM, Sisseln, Switzerland). Fresh diets were provided every week, and body weight was monitored at that point. Average food consumption of WT, *Bco2*$^{-/-}$,and *Isx*$^{-/-}$/*Bco2*$^{-/-}$ mice was estimated by measuring the leftover food from the cage divided by the number of mice present in the cage. Fecal matter collection for mice on either 50 mg/kg 3R,3′R-zeaxanthin, or 250 mg/kg 3R,3′R-zeaxanthin occurred at several time points (0, 1, 2, 4, 7, 14, 21, and 28 days). At the end of the experimental period, mice were anesthetized as described above. The tissues were immediately dissected, weighed, and snap-frozen in liquid nitrogen, and stored at −80 °C until further analysis.

2.4. Light exposure experiments

Albino *Isx*$^{-/-}$/*Bco2*$^{-/-}$ mice were used for the light experiment. Immediately after weaning, albino *Isx*$^{-/-}$/*Bco2*$^{-/-}$ mice were placed on either a 250 mg/kg 3R,3′R-zeaxanthin diet or a control diet for 4 weeks. Each dietary group was then separated into three experimental cohorts. These included 1) dark-condition, 2) dark/light-condition, and 3) light-stressed experimental groups. Mice in the dark-condition group were housed in a dark room for 24 h/day for 4 weeks. Those in the dark/light-condition group were housed in the standard mouse facility with a 12/12-hour light/dark cycle. Mice in the light-stress group were housed under the same conditions as the dark/light-condition group, however, they were exposed to light stress twice a week starting at the second week of dietary supplementation and ending after 4 weeks of supplementation. Mice were dark-adapted overnight before light treatment. Immediately prior to light treatment, mice pupils were dilated with 1% tropicamide (Falcon Pharmaceuticals, Fort Wort, TX, USA). Light stress was induced in mice by white light exposure at 85,000 lux (100 W LED Floodlight; MoS Lighting Technology Co., Ltd, Shenzhen, China) for 2 min in a white bucket. Mice were then returned to normal husbandry conditions with a 12/12-hour light/dark cycle.

2.5. Carotenoid extraction

Carotenoid extraction from tissues was performed under dim red light (<600 nm). Carotenoids were extracted from ~25 mg of the liver, duodenum, jejunum, ileum, white adipose tissue, fecal matter, 100 uL of serum, and one whole eye as previously described [24,31]. Briefly, tissues were dissolved and homogenized in 200 uL of PBS. This was followed by the addition of 200 uL methanol, 400 uL acetone, 200 uL diethyl ether, and 400 uL hexane to extract carotenoids. Phase separation was achieved by centrifugation at 4000×*g* for 30 s. The organic phase was collected and the extraction was repeated. The combined organic phases were collected and dried in a SpeedVac (Eppendorf, Hauppauge, NY). Extracted carotenoids were dissolved in 150 uL of hexane: ethyl acetate (70:30, v/v) for normal phase HPLC analysis or dissolved in 150 uL of hexane: isopropanol (95:5, v/v) for chiral HPLC analysis.

2.6. HPLC and LC-MS analysis

Two HPLC methods were employed for the analysis of extracted carotenoids. Method 1 determined carotenoid content via HPLC analysis performed on a 1200 Agilent HPLC series equipped with a diode array detector and normal-phase Agilent Zorbax silica column (4.6 mm ID x 150 mm with 5 mm packing; Agilent, Santa Clara, CA). Chromatographic separation was achieved with an isocratic flow of 30% ethyl acetate in hexane at a flow rate of 1.4 mL/min. The system was scaled with known amounts of authentic 3R, 3′R-zeaxanthin received from DSM (Sisseln, Switzerland). Method 2 involved the separation of chiral metabolites from tissues. A chiral column, ChiralPak AD (Daicel Technologies, West Chester, PA USA), of 25 cm length × 4.6 mm internal diameter was used. Chromatographic separation was achieved with an isocratic flow of 5% isopropanol in hexane at a flow rate of 1 mL/min. The system was calibrated with known amounts of authentic 3R,3′R-zeaxanthin, 3R,3′S-zeaxanthin, and 3S, 3′S-zeaxanthin, which were received from DSM (Sisseln, Switzerland). Oxidized zeaxanthin metabolites were identified based on their retention time, spectra characteristics, and molecular masses. This was achieved by first performing thin-layer chromatography (TLC) using liver tissue samples to separate the different metabolites. Subsequently, individual bands from the TLC plate were isolated and separated on a chiral column as described above. Liquid chromatography-mass spectrometry (LC/MS) analysis was performed using LTQ linear ion trap mass spectrometer equipped with an atmospheric pressure chemical ionization probe (Thermo Fisher Scientific). Chromatographic conditions were the same as described above. MS signal acquisition was performed in positive ionization mode and the MS parameters were optimized for zeaxanthin.

2.7. β-galactosidase expression staining

WT and *Bco2*$^{-/-}$ jejunum were harvested in cold PBS and were immediately frozen individually in OCT compound (Sakura) on dry ice. Frozen tissues were sectioned at 10 microns and cut slides were stored at −80 °C until staining. Immediately prior to staining, slides were fixed in slide fixative (0.2% glutaraldehyde in PBS) for 10 min on ice. Slides were first washed in PBS for 10 min, followed by 10 min of washing with detergent rinse (0.02% Igepal, 0.01% Sodium Deoxycholate, and 2 mM $MgCl_2$ in 0.1 M phosphate buffer [pH 7.5]). Slides were then covered with 1 mg/mL X-gal staining solution for 2 h at 37°C in the dark. Slides were post-fixed in 4% PFA (4% Paraformaldehyde [PFA] in PBS) for 10 min. Following this, slides were rinsed in PBS for 10 min and underwent two washes in distilled water for 5 min each. Counter-stain with Nuclear Fast Red (Vector Laboratories) was done for 5 min and rinsed with distilled water twice and washed in distilled water for 2 min. Slides were dehydrated with grades of ethanol in xylene (50, 70, 90, and 100%) and two changes of xylene and mount with Permount and coverslip.

2.8. Western blotting

Total protein was extracted from mice. Recombinant *β-galactosidase* supernatant (0.15 μg of protein) was used as a positive control in the β-galactosidase Western blot. Following extraction, proteins (30 μg) were separated on 10% SDS-PAGE gels using the Bio-Rad Mini gel system and transferred onto polyvinylidene fluoride (PVDF) membranes (Roche, Basel, Switzerland). After transfer, PVDF membranes were blocked with 5% skim milk prepared in Tris-buffered saline (pH 7.4) containing 0.1% Tween (TBS-T) for 1 h. Membranes were then probed with an anti-β-galactosidase antibody (Proteintech Group, Illinois, USA, catalog number 14323-1-AP) or SR-B1 antibody (Abcam, Cambridge, UK) at a dilution of 1:1,000 overnight at 4°C. After washing with TBS-T, membranes were incubated with the appropriate horseradish peroxidase-conjugated secondary antibody at the dilution of 1:10,000. Blots were washed and detected with CL chemiluminescence substrate according to manufacturer instructions (Thermo Fisher Scientific, Waltham, MA).

2.9. Optical coherence tomography (OCT)

Albino *Isx*$^{-/-}$*/Bco2*$^{-/-}$ mice pupils were dilated with 1% tropicamide (Falcon Pharmaceuticals, Fort Wort, TX, USA). Following this, mice were anesthetized with an intraperitoneal injection of a cocktail of 20 mg/mL ketamine and 1.75 mg/mL xylazine. Mice whiskers were trimmed to avoid image artifacts. Spectral-domain (SD)-optical coherence tomography (SD-OCT) images were acquired in the linear B-scan mode of an ultra-high-resolution SD-OCT instrument (Bioptigen, Morrisville, NC, USA) as previously described [32].

2.10. Electroretinography (ERG)

Prior to performing ERG, supplemented albino *Isx*$^{-/-}$*/Bco2*$^{-/-}$ mice were dark-adapted overnight. Mice pupils were dilated with 1% tropicamide (Falcon Pharmaceuticals, Fort Wort, TX, USA). Following this, mice were anesthetized with an intraperitoneal injection of a cocktail of 20 mg/mL ketamine and 1.75 mg/mL xylazine. Mice were placed on a temperature-regulated heating pad throughout each recording session. Diagnosis Celeris rodent ERG device (Diagnosis, Lowell, MA,USA) with an Ag-AgCL cornea electrode was used for recordings. Scotopic responses were obtained in the dark with 10 steps of white light and flash stimulus, ranging from 0.001 to 20 cd s × m^{-2}. The duration of the inter-stimulus intervals increased from 4 s for low-luminance flashes to 90 s for the highest stimuli. After 7min of light adaptation, cone ERGs were recorded with strobe-flash stimuli (0.32—63 cd s × m^{-2}) superimposed on the adapting field [32].

2.11. Real-time quantitative PCR analyses

WT mice were sacrificed and tissues were harvested. Total RNA was extracted from tissues by TRIZOL method (Invitrogen, Carlsbad, CA) and quantified using Nanodrop ND-1000 spectrophotometer (Thermo Fisher Scientific, Waltham, MA). cDNA was generated using the High Capacity RNA to cDNA kit (Applied Biosystems, Thermo Fisher Scientific, Waltham, MA, USA). Gene expression measurement was carried out by real-time quantitative PCR using an Applied Biosystems Real-Time PCR instrument with Taq Man probes (Applied Biosystems; Thermo Fisher Scientific, Waltham, MA, USA). Primers used were *β-actin* (Mm02619580) and *Bco2* (Mm00460048). Amplification was carried out using TaqMan polymerase. Fast Universal PCR Master Mix (2 ×) No Amp Erase, UNG (Applied Biosystems; Thermo Fisher

Scientific, Waltham, MA, USA) following the manufacturer's protocol. 10 ng cDNA was used per 10 μL reaction. Gene expression levels were normalized to the expression of housekeeping gene *β-actin* using the ΔΔCt method as previously described [33].

2.12. Statistical analysis

Statistical analyses were performed using unpaired Student's *t*-test and one-way ANOVA using GraphPad Prism 8.0 software (GraphPad). An alpha level of $P < 0.05$ was considered significant. Data are expressed as mean values ± standard deviation.

3. RESULTS

3.1. BCO2 is expressed in high levels in enterocytes of the mouse intestine

The exact physiological role of BCO2 in mammals is not fully elucidated. Therefore, to characterize BCO2 in murine carotenoid metabolism, we first examined its mRNA expression within multiple tissues from wild-type (WT) mice maintained on a normal chow diet. RT-qPCR was performed and normalized to the housekeeping gene *β-actin*. To identify tissues with the highest expression, fold change values were plotted in decreasing order based on the tissue with the highest fold change (Figure 1A). The highest *Bco2* expression within WT mice was observed in the duodenum of the small intestine. Other tissues that exhibited high mRNA levels of *Bco2* were the liver, kidney, testis, and jejunum. In contrast, the adrenal gland, spleen, and lymph node exhibited low *Bco2* mRNA levels.

The lack of a BCO2-specific antibody prevents the analysis of BCO2 expression on the protein level [31]. To circumvent this problem, we utilized a previously established *Bco2* $^{-/-}$ mouse model [29]. In this transgenic mouse line, exons 1 to 4 of the murine *Bco2* gene were deleted and replaced with a *lacZ* reporter gene that is expressed under the control of the native murine *Bco2* promoter (Figure. S1A). The *lacZ* gene contains a nuclear target sequence that results in the nuclear transport of the encoded β-galactosidase. We first confirmed β-galactosidase expression by Western blotting using total protein isolated from the liver, duodenum, jejunum, and ileum of *Bco2*$^{-/-}$ mice (Figure. S1B). The β-galactosidase antibody detected a band that co-migrated with a bacterial β-galactosidase on the SDS-PAGE (Figure. S1B). To examine which small intestine cell types BCO2 is expressed, we performed a β-galactosidase staining assay with cross sections of the jejunum isolated from either *Bco2*$^{-/-}$ or WT mice. This assay revealed strong blue staining of the nuclei of enterocytes along the microvilli of the intestinal lining of *Bco2*$^{-/-}$ mice (Figure. 1B). This blue staining was absent in WT control mice, indicating that the staining was specific for recombinant β-galactosidase expression and activity.

The high expression of BCO2 in the intestine suggested that the enzyme converts carotenoids upon absorption into apocarotenoids. To test this hypothesis, we supplemented WT mice with a high dose of zeaxanthin (250 mg/kg diet). After a four-week dietary intervention, we sacrificed the mice and determined via high-pressure liquid chromatography (HPLC) analysis the zeaxanthin concentrations in different tissues. As previously reported, we detected parent zeaxanthin as well as oxidized metabolites [29]. In the intestine, the lowest concentration of zeaxanthin existed in the duodenum with the highest *Bco2* expression (Figure 1A &C). The jejunum contained the highest amount of zeaxanthin, in which the major metabolite again was the parent

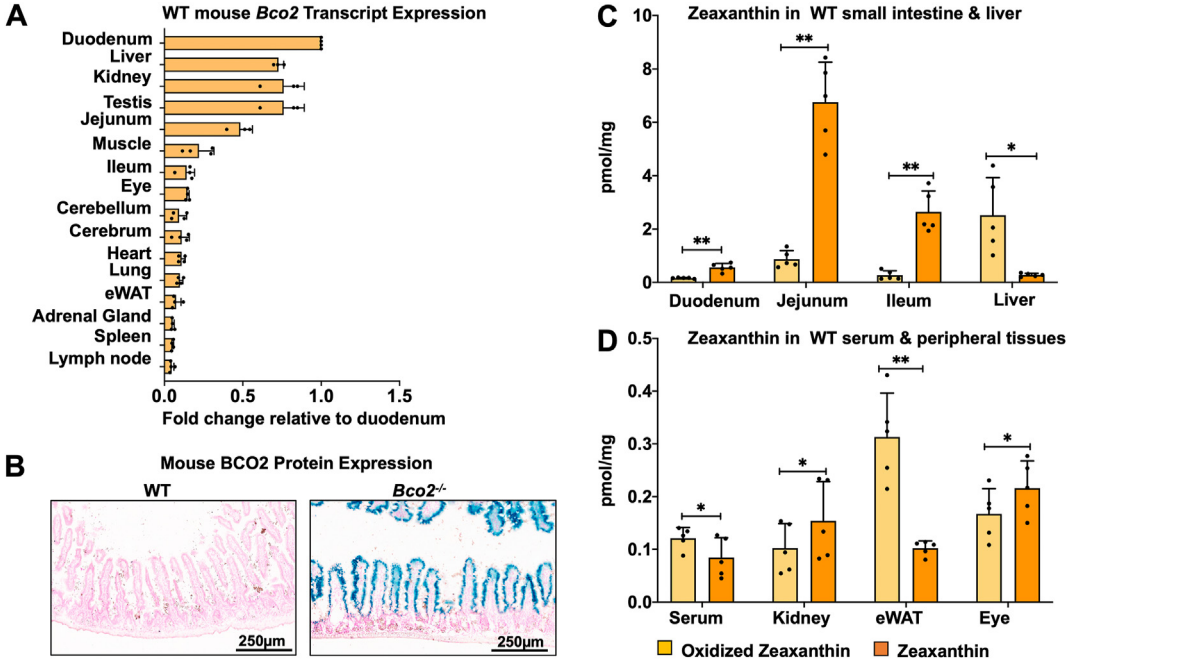

Figure 1: *Bco2* gene expression profile and zeaxanthin metabolites in WT mice. A) Mouse *Bco2* mRNA expression in various tissue from WT mice (n = 4) maintained on a normal chow diet. Total RNA was extracted from various tissues and RT-qPCR was performed to determine the tissue transcript expression pattern of *Bco2*. **B)** Staining for β-galactosidase in WT and *Bco2*$^{-/-}$ small intestine. In *Bco2*$^{-/-}$ mice, β-galactosidase is expressed and serves as a BCO2 reporter. β-galactosidase staining was performed on cross-sections of the jejunum from the small intestine of *Bco2*$^{-/-}$ and WT mice (negative control). Blue staining is observed in enterocytes of the villi of *Bco2*$^{-/-}$ mice. **C-D)** Quantification of oxidized zeaxanthin (yellow) and parent zeaxanthin (orange), from WT mice tissues. WT mice (n = 5) were supplemented with 250 mg/kg zeaxanthin for 4 weeks. Zeaxanthin metabolites were isolated from harvested tissues and quantified via HPLC analysis. **C)** Oxidized zeaxanthin (yellow) and zeaxanthin (orange) from the duodenum, jejunum, Ileum, and liver in WT mice. **D)** Oxidized zeaxanthin (yellow) and zeaxanthin (orange) from serum, kidney, epididymal white adipose tissue (eWAT), and eye of WT mice. Values indicate means ± SD. Statistical analyses were performed by comparing tissues using unpaired two-tailed Student's *t*-test. $^{*}P < 0.05$; $^{**}P < 0.01$. Statistical significance was determined using Prism 8 software, with a significance threshold set at $P < 0.05$.

compound (Figure. 1C). In contrast to the jejunum, the liver contained mostly oxidized zeaxanthin. The concentration of zeaxanthin metabolites was about 40-fold lower in the serum, eyes, and kidney of WT mice (Figure. 1D). In epididymal white adipose tissue (eWAT), that serves as a reservoir for lipids, a slightly higher concentration of zeaxanthin existed in comparison to the kidney and the eye (Figure. 1D). Thus, we observed that zeaxanthin was absorbed as shown by its high intestinal concentration but high BCO2 expression in the intestine and liver (Figure. 1A) led to its rapid metabolic turnover and prevented accumulation in the body.

3.2. The transcription factor ISX determines zeaxanthin bioavailability in mice

SR-B1 facilitates the uptake of carotenoids and other fat-soluble vitamins in the enterocytes of the intestine [34]. Mice deficient for the transcription factor ISX display increased SR-B1 expression in distal parts of the intestine [35–37]. We used *Bco2*$^{-/-}$ and *Isx*$^{-/-}$*/Bco2*$^{-/-}$ mice to test the effects of ISX deficiency for zeaxanthin absorption in mice [35]. To determine the effects of BCO2 and ISX on carotenoid metabolism, 4-week-old *Bco2*$^{-/-}$ *and Isx*$^{-/-}$*/Bco2*$^{-/-}$ mice were placed on diets containing increasing concentrations of zeaxanthin (0 mg/kg, 50 mg/kg, and 250 mg/kg) (Figure 2A). We chose the supraphysiological supplementation (250 mg/kg) to test whether we can saturate zeaxanthin uptake in the mouse gut.

The dietary intervention with zeaxanthin did not affect food intake in *Bco2*$^{-/-}$ and *Isx*$^{-/-}$*/Bco2*$^{-/-}$ mice (Figure. S2A). During the intervention, we collected the fecal matter to compare zeaxanthin absorption in *Bco2*$^{-/-}$ and *Isx*$^{-/-}$*/Bco2*$^{-/-}$ mice. Fecal matter collection occurred over 28 days of the dietary intervention at several time points (0, 1, 2, 4, 7, 14, 21, and 28 days). We performed HPLC analysis to determine zeaxanthin content within the fecal matter. At 50 mg/kg zeaxanthin supplementation, *Isx*$^{-/-}$*/Bco2*$^{-/-}$ mice excreted less zeaxanthin than *Bco2* $^{-/-}$ mice, indicative of enhanced absorption (Figure. S2C). The difference between the genotypes was more pronounced at the beginning of the dietary intervention. During the four weeks of intervention, the amount of excreted zeaxanthin decreased in *Bco2*$^{-/-}$ mice and converged to the levels of *Isx*$^{-/-}$*/Bco2*$^{-/-}$ mice (Figure. S2C). In the cohort of mice supplemented with 250 mg/kg of zeaxanthin, *Isx*$^{-/-}$*/Bco2*$^{-/-}$ mice also excreted less zeaxanthin than *Bco2*$^{-/-}$ mice though the difference between the genotypes was less pronounced than on the 50 mg/kg zeaxanthin diet (Figure. S2E). Interestingly, we observed under all dietary conditions the excretion of some oxidized zeaxanthin (Figure 2B and D) though its levels in the feces were far lower than parent zeaxanthin.

After 4 weeks of dietary intervention, we sacrificed mice and collected tissues. The modulation of carotenoid absorption by the *Isx* genotype was visibly observable by the color of adipose tissues. Isolated eWAT from mice on either 50 mg/kg or 250 mg/kg zeaxanthin was yellow in *Bco2*$^{-/-}$ mice and orange in *Isx*$^{-/-}$*/Bco2*$^{-/-}$ mice (Figure. 2B). This yellow coloration was more pronounced in the adipose tissue of *Isx*$^{-/-}$*/Bco2*$^{-/-}$ in comparison to *Bco2*$^{-/-}$ mice (Figure. 2B). Quantification of the total carotenoid content of eWAT confirmed that *Isx*$^{-/-}$*/Bco2*$^{-/-}$ mice accumulated significantly higher amounts of zeaxanthin than *Bco2*$^{-/-}$ mice under either dietary condition (Figure. 2C). Thus,

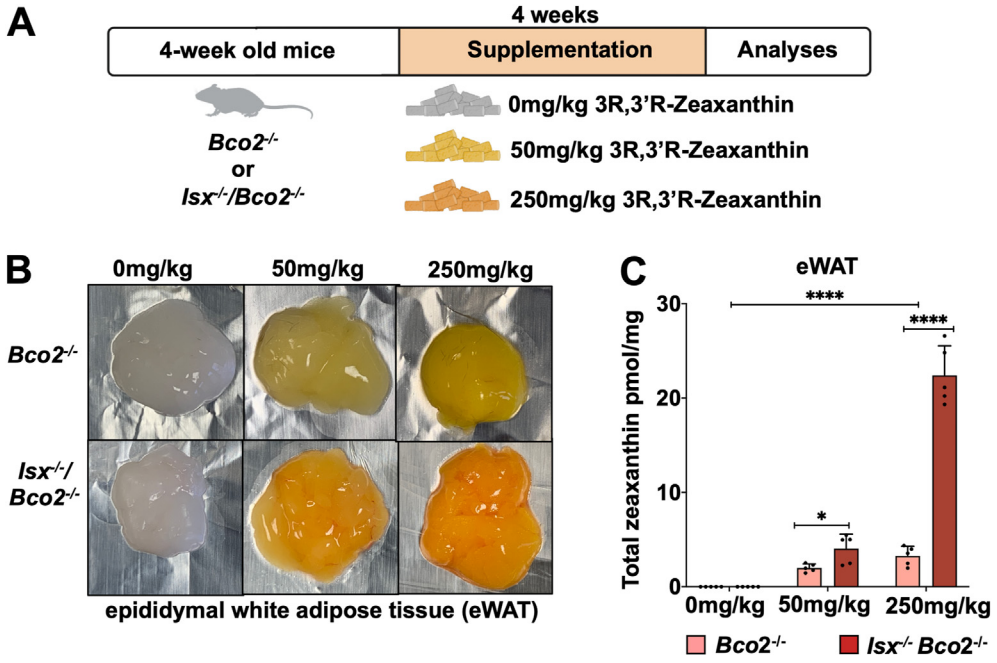

Figure 2: Yellow fat phenotype of *Bco2*$^{-/-}$ and *Isx*$^{-/-}$*/Bco2*$^{-/-}$ mice. A) Scheme of dietary zeaxanthin supplementation of *Bco2*$^{-/-}$ and *Isx*$^{-/-}$*/Bco2*$^{-/-}$ mice. Immediately after weaning, mice were placed on either a control diet of 0 mg/kg zeaxanthin, 50 mg/kg zeaxanthin, or 250 mg/kg zeaxanthin diet for 4 weeks followed by tissue analysis. **B)** Photographs of eWAT harvested from *Bco2*$^{-/-}$ and *Isx*$^{-/-}$*/Bco2*$^{-/-}$ mice under different supplementation conditions. **C)** HPLC quantification analysis of total zeaxanthin (pmol/mg) from eWAT of *Bco2*$^{-/-}$ and *Isx*$^{-/-}$*/Bco2*$^{-/-}$ mice under different supplementation conditions. Values indicate means ± SD from five mice (3 females and 2 males) per tissue. Statistical analyses were performed by comparing tissues using two-way ANOVA. $^{*}P < 0.05$; $^{**}P < 0.005$, $^{***}P < 0.0001$. Statistical significance for oxidized and parent zeaxanthin between different dietary groups was analyzed using an unpaired two-tailed Student's *t*-test. $^{*}P < 0.05$, $^{**}P < 0.01$, $^{***}P < 0.001$, $^{****}P < 0.001$. Statistical significance was determined using Prism 8 software, with a significance threshold set at $P < 0.05$.

zeaxanthin was absorbed in a concentration-dependent manner and this absorption increased when the suppressive regulatory effect of ISX was removed by genetic dissection.

3.3. Zeaxanthin absorption in mice occurs in the jejunum

We next compared the protein levels of SR-B1 in the intestine (duodenum, jejunum, and ileum) of mice of different genotypes supplemented with 250 mg/kg zeaxanthin (Figure. S3). SR-B1 expression was high in the duodenum and jejunum of *Isx*$^{-/-}$/*Bco2*$^{-/-}$ mice when compared to *Bco2*$^{-/-}$ and WT mice. To compare the effect of the *Isx* genotype on zeaxanthin absorption and body distribution, we determined zeaxanthin levels in *Bco2*$^{-/-}$ and *Isx*$^{-/-}$/*Bco2*$^{-/-}$ mice maintained under different dietary conditions. HPLC analysis was performed to identify and quantify zeaxanthin and its metabolites. Again, HPLC traces displayed oxidized zeaxanthin and parent zeaxanthin (Figure. S4A). The presence of oxidized zeaxanthin metabolite was observed in the duodenum, jejunum, and ileum of both genotypes at both the low (50 mg/kg) and high (250 mg/kg) concentrations of zeaxanthin supplementation (Figure 3). The overall zeaxanthin concentration was increased in all parts of the intestine of *Isx*$^{-/-}$/*Bco2*$^{-/-}$ mice when compared to *Bco2*$^{-/-}$ mice (Figure 3A–C & 3E-G). In *Isx*$^{-/-}$/*Bco2*$^{-/-}$ mice, the duodenum, jejunum, and ileum displayed higher concentrations of the oxidized zeaxanthin when compared to the parent zeaxanthin at 50 mg/kg of zeaxanthin (Figure 3E–G). The same distribution was observed in the duodenum and the ileum but not the jejunum of *Bco2*$^{-/-}$ mice at 50 mg/kg zeaxanthin (Figure 3A–C). At 250 mg/kg zeaxanthin supplementation, there was no significant differences between oxidized and parent zeaxanthin in the duodenum and ileum of the *Isx*$^{-/-}$/*Bco2*$^{-/-}$ mice (Figure 3E,G). However, the jejunum exhibited a far higher amount of parent zeaxanthin than oxidized zeaxanthin under this supply condition (Figure. 3F). The same patterns were observed in the *Bco2*$^{-/-}$ mice though the overall concentration of zeaxanthin and oxidized zeaxanthin were lower than in the double mutant (Figure 3A–H).

In intestinal enterocytes, carotenoids are packaged in lipoproteins, secreted in the circulation, and eventually taken up by the liver [34]. Therefore, we next determined concentrations of hepatic zeaxanthin in the different mouse strains. Again, we observed a dose-dependent increase of zeaxanthin in both genotypes (Figure 3D &H). At 50 mg zeaxanthin, only the oxidized form of zeaxanthin became detectable. At 250 mg zeaxanthin, the oxidized form was the prevalent form but also significant amounts of parent zeaxanthin were detectable. The hepatic concentration of zeaxanthin metabolites was 3-fold higher in *Isx*$^{-/-}$/*Bco2*$^{-/-}$ than in *Bco2*$^{-/-}$ mice (Figure 3D &H). However, there was no significant difference in liver weight between the different dietary groups in *Bco2*$^{-/-}$ and *Isx*$^{-/-}$/*Bco2*$^{-/-}$ mice (Figure. S5). Moreover, the hepatic concentration exceeded the intestinal concentrations.

Taken together, we observed a dose-dependent increase in zeaxanthin concentrations in all parts of the intestine of the two mouse mutants. The highest concentration of zeaxanthin and its oxidized metabolite was found in the jejunum in both mouse genotypes. However, the data also highlighted significant differences between *Bco2*$^{-/-}$ and *Isx*$^{-/-}$/*Bco2*$^{-/-}$ mice. The *Isx*$^{-/-}$/*Bco2*$^{-/-}$ mice displayed far higher levels

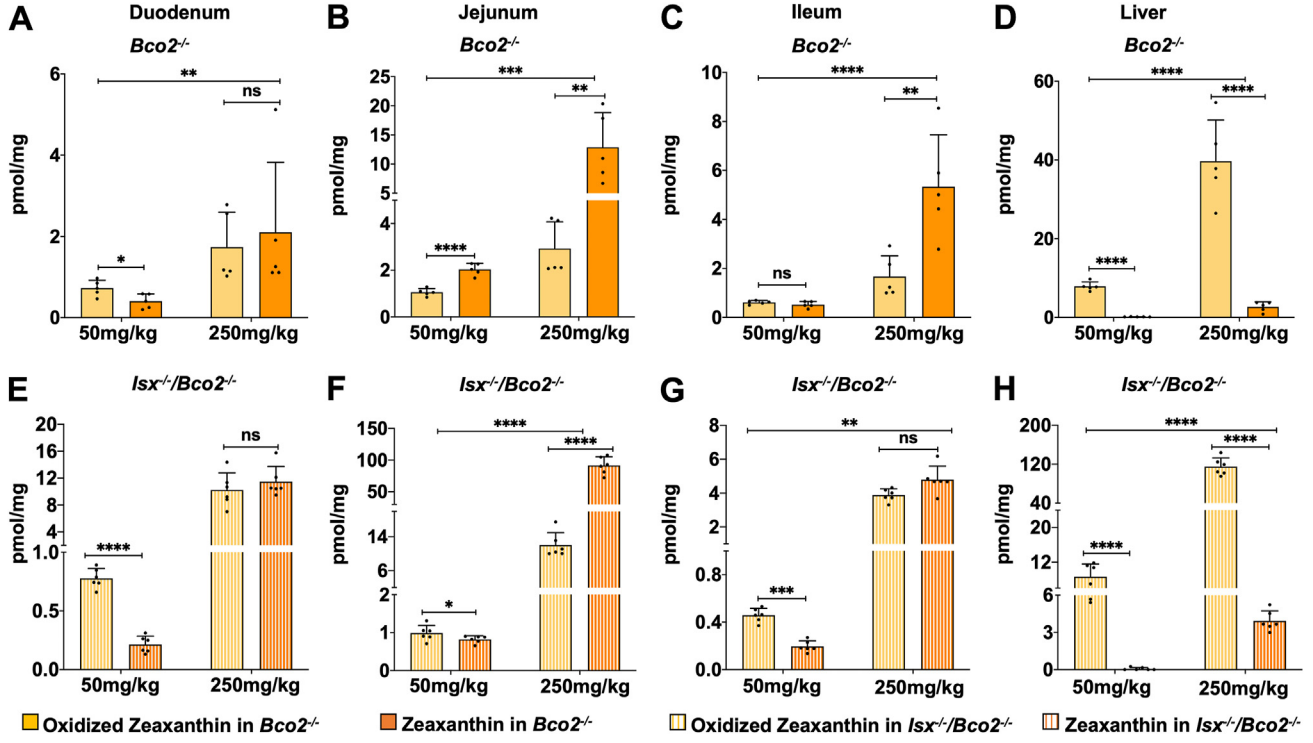

Figure 3: Concentrations of oxidized and parent zeaxanthin in the small intestine and liver of *Bco2*$^{-/-}$ and *Isx*$^{-/-}$/*Bco2*$^{-/-}$ mice. A-H) HPLC quantification of oxidized zeaxanthin (yellow) and parent zeaxanthin (orange) of duodenum (A & E), jejunum (B & F), Ileum (C & H), and liver (D & H) of *Bco2*$^{-/-}$ (solid bars) **(A–D)** and *Isx*$^{-/-}$/*Bco2*$^{-/-}$ (patterned bars) **(E–H)** mice. Values indicate means ± SD from five (2 females and 3 males) *Bco2*$^{-/-}$ mice or six (3 females and 3 males) *Isx*$^{-/-}$/*Bco2*$^{-/-}$ mice per tissue. Statistical analyses were performed by comparing tissues using two-way ANOVA. $^{*}P < 0.05$; $^{**}P < 0.005$, $^{***}P < 0.0001$. Statistical significance for oxidized and parent zeaxanthin between different dietary groups was analyzed using an unpaired two-tailed Student's t-test. $^{*}P < 0.05$, $^{**}P < 0.01$, $^{***}P < 0.001$, $^{****}P < 0.001$. Statistical significance was determined using Prism 8 software, with a significance threshold set at $P < 0.05$.

of zeaxanthin metabolites than *Bco2*$^{-/-}$ mice in all parts of the intestine and the liver. Additionally, the ratio of oxidized to parent zeaxanthin was influenced by the amount of zeaxanthin supplementation, indicating that the oxidation process is saturable when increased amounts of zeaxanthin are provided via the diet.

3.4. Concentration and ratio of oxidized to non-oxidized zeaxanthin metabolites in serum and selected peripheral tissues

To determine the zeaxanthin metabolite profile of the serum, eWAT, kidney, and eye, tissues were harvested from *Bco2*$^{-/-}$ and *Isx*$^{-/-}$/*Bco2*$^{-/-}$ mice. HPLC analysis was performed to identify and quantify zeaxanthin metabolites (Figures. 4 & S4B). A pattern that emerged in serum and the selected peripheral tissues was that at 50 mg/kg zeaxanthin, the concentration of oxidized zeaxanthin was significantly higher than that of the parent compound (Figure 4). The concentration of carotenoids was similar in kidney and serum, whereas the concentration was two-fold higher in eWAT and the eyes of *Bco2*$^{-/-}$ and *Isx*$^{-/-}$/*Bco2*$^{-/-}$ mice.

At 250 mg/kg zeaxanthin, oxidized zeaxanthin was still the prevalent metabolite (approx.10: 1 ratio) in the serum of *Isx*$^{-/-}$/*Bco2*$^{-/-}$ and *Bco2*$^{-/-}$ mice (Figure 4A & E). The same result was found in eWAT though the carotenoid concentration was higher than in serum (Figure 4A,C & 4E, G). In contrast, the kidney and eyes of *Isx*$^{-/-}$/*Bco2*$^{-/-}$ mice exhibited ratios of respectively ~3:1 and 1.5:1 of oxidized to parent zeaxanthin at 250 mg/kg zeaxanthin (Figure 4F & H). The same trend was observed in *Bco2*$^{-/-}$ mice though the carotenoid concentration was lower than in the double mutant (Figure 4B & D). Thus, the ratio of oxidized to parent zeaxanthin within peripheral tissues was dose-dependent and variable between tissues.

3.5. Characterization of zeaxanthin metabolites

The liver contained mostly oxidized zeaxanthin and we utilized liver samples of *Isx*$^{-/-}$/*Bco2*$^{-/-}$ mice to determine its exact chemical nature. We first performed preparative thin-layer chromatography (TLC) with hepatic lipid extracts based on polarity using silica plates. After the development of the plate, three distinct yellow bands were observed (Figure 5A inset). Band 1 was the most prominent, indicating that it contains the prevalent metabolite. The bands were scraped from the silica plate and the carotenoids were extracted. The extracts were analyzed by HPLC on a chiral column because zeaxanthin and its oxidized metabolites exist in various enantiomers. Additionally, we subjected the carotenoids to mass spectrometry analysis. With this approach, different zeaxanthin metabolites were identified and characterized based on retention time, spectral characteristics, and molecular mass. Before the analysis, the chiral column was gauged by a mixture of zeaxanthin enantiomer standards, including 3R,3′R, 3R,3′S, and 3S, 3′S-zeaxanthin (Figure. S6). Chiral HPLC analysis revealed that band 1 contained three major peaks (peaks 1, 2, and 3) (Figure. 5A). Peak 1 had a retention time of 18.8 min, peak 2 had a retention time of 20.4 min, and peak 3 had a retention time of 22.5 min. Two metabolites (peaks 8 and 9) were present in band 3. Peak 8 had a retention time of 23.9 min and peak 9 had a retention time of 26.0 min. The faintness of band 2 on the TLC plate suggested that it is a minor metabolite and its low absorbance value on the HPLC trace confirmed this assumption (Figure. 5A). Band 2 contained four metabolites (peaks 4, 5, 6, & 7). Peaks 4, 5, 6, and 7 had retention times of 18, 19.9, 22.4, and 28 min, respectively. Spectroscopic analyses revealed that peaks 1, 2, and 3 shared identical characteristics (Figure. 5B). Additionally, monoisotopic molecular ions for peaks 1, 2, and 3 were 565.5 $[MH]^+$,

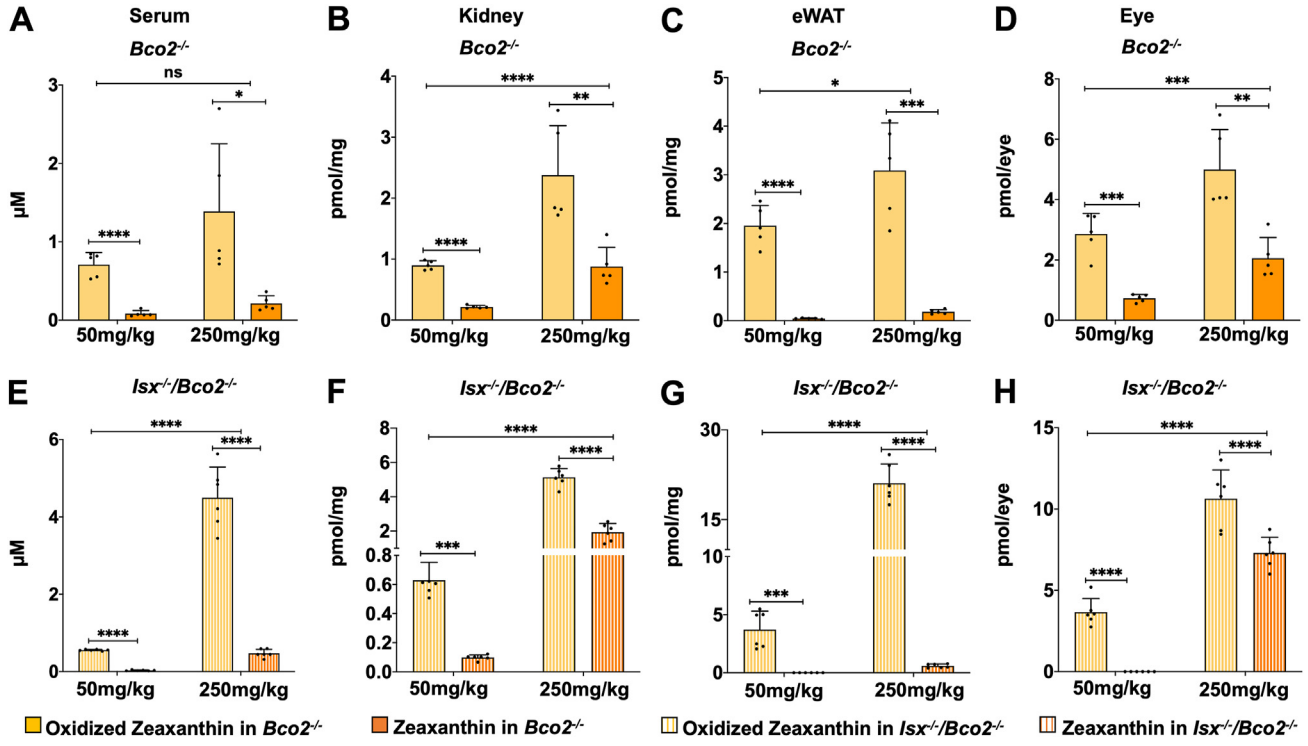

Figure 4: Peripheral tissues exhibit different oxidized and parent zeaxanthin ratios in *Bco2*$^{-/-}$ and *Isx*$^{-/-}$/*Bco2*$^{-/-}$ mice. A-H) HPLC quantification of oxidized zeaxanthin (yellow) and parent zeaxanthin (orange) in serum (A & E), kidney (B & F), eWAT (C & H), and eye (D & H) of *Bco2*$^{-/-}$ (solid bars) **(A–D)** and *Isx*$^{-/-}$/*Bco2*$^{-/-}$ (patterned bars) **(E–H)** mice. Values indicate means ± SD from five (2 females and 3 males) *Bco2*$^{-/-}$ mice or six (3 females and 3 males) *Isx*$^{-/-}$/*Bco2*$^{-/-}$ mice per tissue. Statistical analyses were performed by comparing tissues using two-way ANOVA. $^{*}P < 0.05$; $^{**}P < 0.005$, $^{***}P < 0.0001$. Statistical significance for oxidized and parent zeaxanthin between different dietary groups was analyzed using an unpaired two-tailed Student's *t*-test. $^{*}P < 0.05$, $^{**}P < 0.01$, $^{***}P < 0.001$, $^{****}P < 0.001$. Statistical significance was determined using Prism 8 software, with a significance threshold set at $P < 0.05$.

565.6 $[MH]^+$, and 565.60 $[MH]^+$ respectively (Figure. S7A—C). A molecular mass of 564.8 corresponds to ε,ε-carotene 3, 3′-dione due to the oxidation of the hydroxyl group and the loss of hydrogen at C3 and C3′ positions of the parent compound, 3R, 3′R-zeaxanthin (Figure. S7F). The identical masses and spectra characteristics but different chiral HPLC retention times of peaks 1, 2, and 3 indicated that these compounds are stereoisomers with chiral centers at the C6 and C6′ positions. Peaks 8 and 9 showed different spectral characteristics and chiral HPLC retention time but had identical masses (Figure 5F—G & S7D-E). Peak 8 had a monoisotopic mass of 569.6 $[MH]^+$ and peak 9 had a mass of 569.6 $[MH]^+$. The molecular mass of 3R,3′R-zeaxanthin is 568.9. Chiral HPLC analysis of pure 3R,3′R-zeaxantin as a standard had a retention time of ∼23 min, which is similar to peak 8's retention time of 23.9 min. Thus, peak 8 corresponded to 3R,3′R-zeaxanthin. The slight difference in spectral characteristics and the later retention time of peak 9 indicated that it may be a cis-isomer of 3R,3′R-zeaxanthin (Figure 5A,G & S7E). We were not able to determine the masses of peaks 4, 5, 6, and 7 because of low abundance but we speculate based on their spectral characteristics that they are zeaxanthin metabolites in which only one ring site underwent oxidation. The production of these compounds has been previously reported in WT mice upon xanthophyll supplementation [38]. We also subjected other tissues to chiral HPLC analysis and determined the presence of zeaxanthin stereoisomers in other tissues, including the eye (Figure 6). All tissues showed similar patterns with ε,ε-carotene 3, 3′-dione (peaks 1, 2, and 3) and 3R, 3′R-zeaxanthin as major zeaxanthin metabolites (Figure. 6). Notably, no peak with a retention time of 3R, 3′S-zeaxanthin was detected in the eyes of the mice (Figures. 6 & S6).

3.6. Albino *Isx*$^{-/-}$/*Bco2*$^{-/-}$ mice serve as a versatile mouse model to study carotenoid biology

We generated an albino *Isx*$^{-/-}$/*Bco2*$^{-/-}$ mice that lack melanin pigmentation to study the light-absorbing properties of carotenoid metabolites. The mice were supplemented with either no zeaxanthin as a control or with 250 mg/kg zeaxanthin for 4 weeks. A striking characteristic of supplemented albino *Isx*$^{-/-}$/*Bco2*$^{-/-}$ mice was the yellow skin color phenotype observed in their ears, eyelids, and nostrils (Figure 7A). This phenotype was not observed in albino *Isx*$^{-/-}$/*Bco2*$^{-/-}$ mice on a control diet. This finding demonstrated that supplementation with high amounts of zeaxanthin can induce hypercarotenemia within these mice. This condition has previously been described in humans with overexposure to carotenoid supplementation [39].

We next performed optical coherence tomography (OCT) and electroretinography (ERG) to determine the effects of carotenoid accumulation in the eyes of these animals. OCT analyses of supplemented and non-supplemented mice revealed no differences in the stratification of the retinal layers (Figure. S8A). There also was no obvious deposition of lipids in the RPE or other retinal layers. ERG analysis revealed normal responses of supplemented and non-supplemented animals under photopic and scotopic conditions (Figure. S8B). Thus, we observed no detrimental effects of zeaxanthin accumulation in the eyes of these mice.

To determine the effects of light absorption on ocular zeaxanthin metabolite concentration and composition, we established an experimental system that exposed albino *Isx*$^{-/-}$/*Bco2*$^{-/-}$ mice to different light conditions. While cohorts of mice were subjected to three distinct light conditions, they were supplemented with either 0 mg/kg or 250 mg/kg zeaxanthin for 4 weeks. One cohort of mice

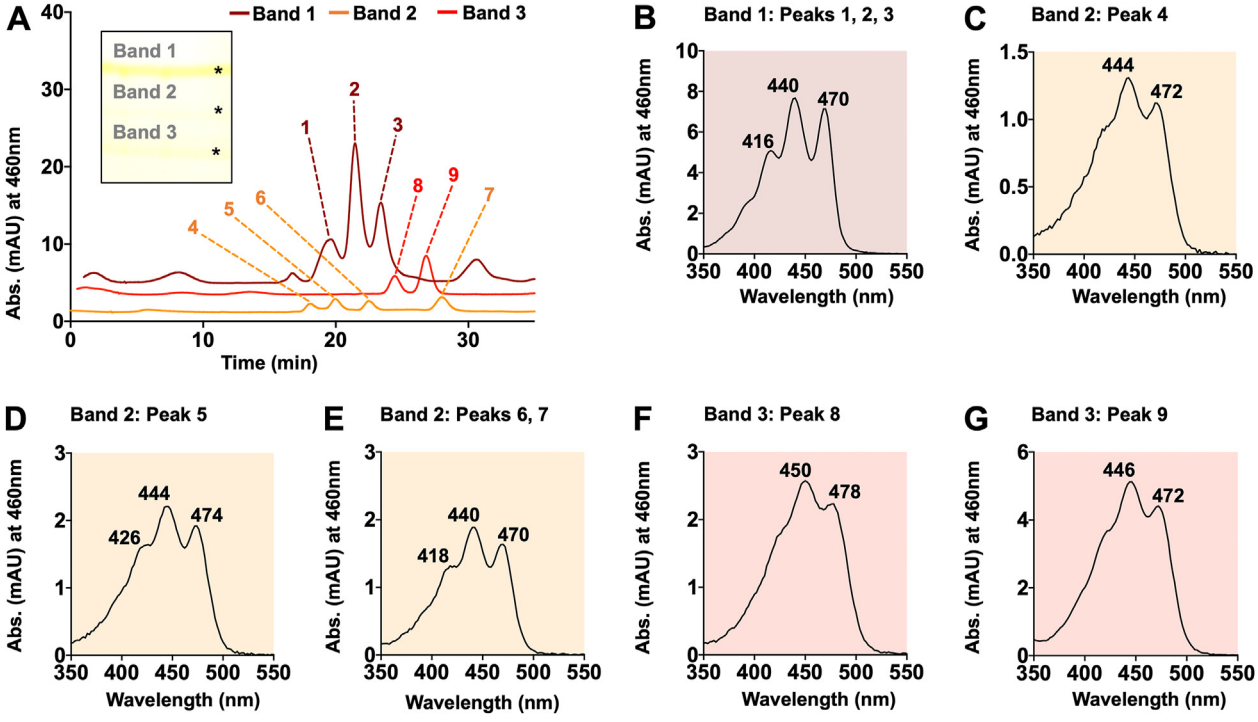

Figure 5: Determination of the chemical nature of zeaxanthin metabolites from *Isx*$^{-/-}$/*Bco2*$^{-/-}$ liver. A) Thin-layer chromatography (TLC) was used to separate hepatic zeaxanthin metabolites extracted from *Isx*$^{-/-}$/*Bco2*$^{-/-}$ mice supplemented with 250 mg/kg zeaxanthin. A photograph of the TLC silica plate showed three distinct bands. Black asterisks indicate the positions of the bands (band 1 = top, band 2 = middle, and band 3 = bottom). Bands were individually scraped from the TLC silica plates, carotenoids were extracted and separated on a chiral HPLC column. Representative chiral HPLC traces at 460 nm of band 1 (burgundy), band 2 (orange), and band 3 (red). Band 1 contains three peaks (peaks 1 (18.8min), 2 (20.4min), and 3 (22.5min)). Band 2 contains four peaks (peaks 4 (18min), 5 (19.9min), 6 (22.4min), and 7 (28min)). Band 3 contains two peaks (peaks 8 (23.9min) and 9 (26.0min)). **B)** Spectral characteristics of peaks 1.2, and 3 from band 1 (burgundy). **C)** Spectral characteristics of peak 4 from band 2 (orange). **D)** Spectral characteristics of peak 5 from band 2 (orange). **E)** Spectral characteristics of peaks 6 and 7 from band 2 (orange). **F)** Spectral characteristics of peak 8 from band 3 (red). **G)** Spectral characteristics of peak 9 from band 3 (red).

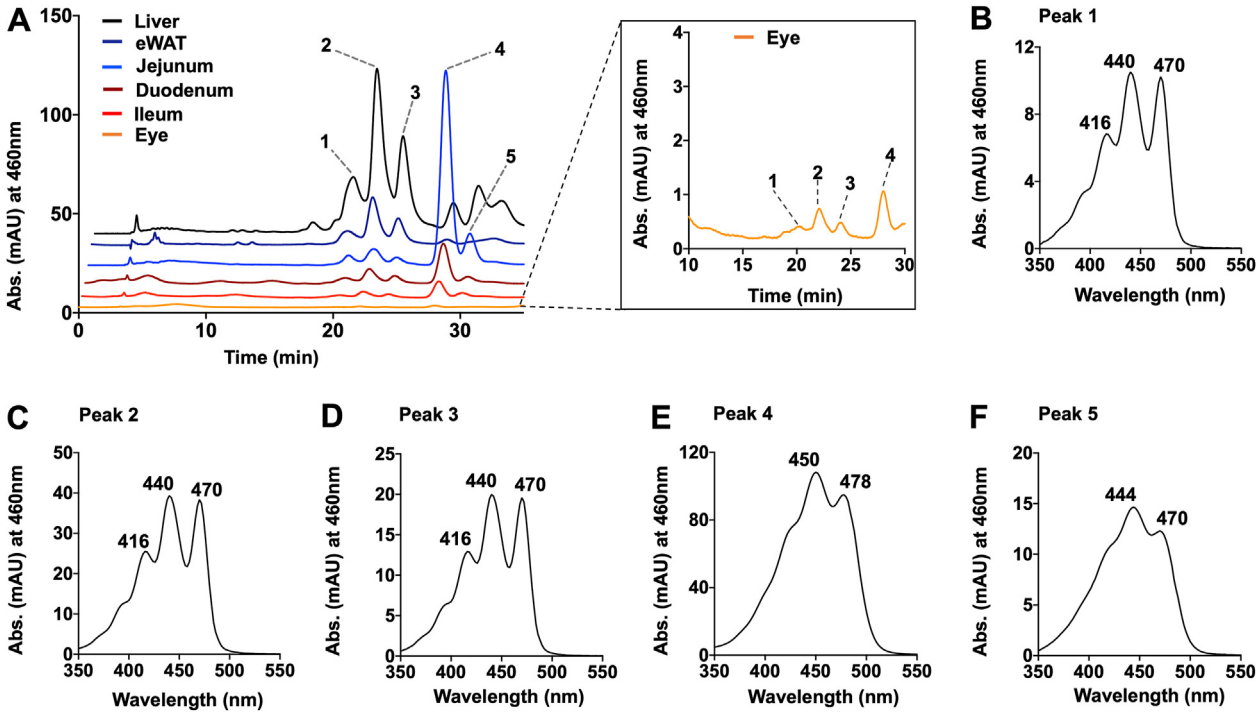

Figure 6: HPLC analysis of zeaxanthin metabolites in mouse tissues. Chiral HPLC analysis was performed with lipid extracts of tissues harvested from *Isx*$^{-/-}$/*Bco2*$^{-/-}$ mice on a 250 mg/kg zeaxanthin diet. **A)** Representative chiral HPLC traces at 460 nm of the liver (black), eWAT (navy), jejunum (blue), duodenum (burgundy), ileum (red), and eye (orange). Peaks 1 (20.5 min), 2 (22.2 min), and 3 (24.2 min) correspond to the three enantiomers of the oxidized zeaxanthin metabolite (ε,ε-carotene-3.3′-dione). Peaks 4 (28.2 min) and 5 (30.2 min) correspond to geometric isomers of 3R,3′R-zeaxanthin. **B)** Spectral characteristics of peak 1. **C)** Spectral characteristics of peak 2. **D)** Spectral characteristics of peak 3. **E)** Spectral characteristics of peak 4. **F)** Spectral characteristics of peak 5.

was housed in darkness (DC group), another cohort was subjected to a light/dark cycle (L/DC group), and a third cohort was subjected to light stress (LS group), at 85,000 lux for 2 min biweekly, while being housed under light/dark cycle condition (Figure. 7B). After four weeks of intervention, we performed HPLC analysis to identify and quantify zeaxanthin metabolites in the eyes. HPLC analysis revealed an increase in the concentration of zeaxanthin metabolites with increasing light exposure (Figure. 7C). Notably, the concentration of oxidized zeaxanthin was increased in the eyes of the L/DC and LS groups when compared to the DC group. While oxidized zeaxanthin increased in a light-dependent manner, the levels of the parent zeaxanthin remained relatively constant between the different groups (Figure. 7D). This light-dependent phenomenon was not observed in the liver of these mice. There was no light-dependent increase of total zeaxanthin or its oxidized form between the different light treatment condition groups (Figure 7E & F). Additionally, the total zeaxanthin amount and the ratio of oxidized to non-oxidized zeaxanthin within the livers were not altered in the groups. There was no significant difference in dietary intake of *Isx*$^{-/-}$/*Bco2*$^{-/-}$ mice subjected to different light conditions (Figure. S9B). Furthermore, OCT and ERG analysis showed no differences in ocular morphology or function between these mice (Figs. S9A and S10).

4. DISCUSSION

Low blood levels of carotenoids are associated with an increased risk of chronic disease states and vitamin A deficiency [8]. Surprisingly, plasma responses to dietary supplementation with these pigments are quite variable between mammalian species [40]. While humans absorb carotenoids efficiently, mice, the most common model in biomedical research, are poor absorbers of the compounds. Genetic studies identified BCO2 and SR-B1 as major determinants of carotenoid tissue levels in animals [34]. We here studied the role of these proteins in murine carotenoid metabolism and used the gained knowledge to establish a humanized mouse model to study the pigments' beneficial and detrimental roles in physiological processes.

Initially, we observed that the intestine, testis, kidneys, and liver displayed the highest *Bco2* mRNA levels from the investigated mice tissues. Within the intestine, we observed a proximal to distal gradient of BCO2 on the protein level. Similar observations were previously made in rats in which the duodenum also showed the highest levels of BCO2 [41,42]. To receive information about which cell types express BCO2 in the intestine, we took advantage of the *lacZ* reporter gene of the *Bco2*$^{-/-}$ mouse strain [29]. Strong β-galactosidase staining was observed in enterocytes of the intestinal villi that was absent in WT mice. Supplementation of WT mice with 250 mg/kg zeaxanthin for 4 weeks resulted in a relatively high accumulation of zeaxanthin in the small intestine with the highest concentration in the jejunum. Some zeaxanthin was detected as oxidized metabolite in the liver of WT mice. By contrast, serum and peripheral tissues displayed far lower concentrations of zeaxanthin and its oxidized metabolites. This observation indicated that intestinal and hepatic expression of BCO2 in mice serves as a gatekeeper of zeaxanthin accumulation in the periphery. Genetic deletion of BCO2 readily diminished the massive first-pass effect in zeaxanthin metabolism and increased its bioavailability. Notably, BCO2 is expressed at very low levels in the human intestine [43,44] and this species-specific expression pattern likely explains its variable bioavailability in rodents and humans. Future studies should focus on the identification of regulatory mechanisms that contribute to this regulation in different mammalian species.

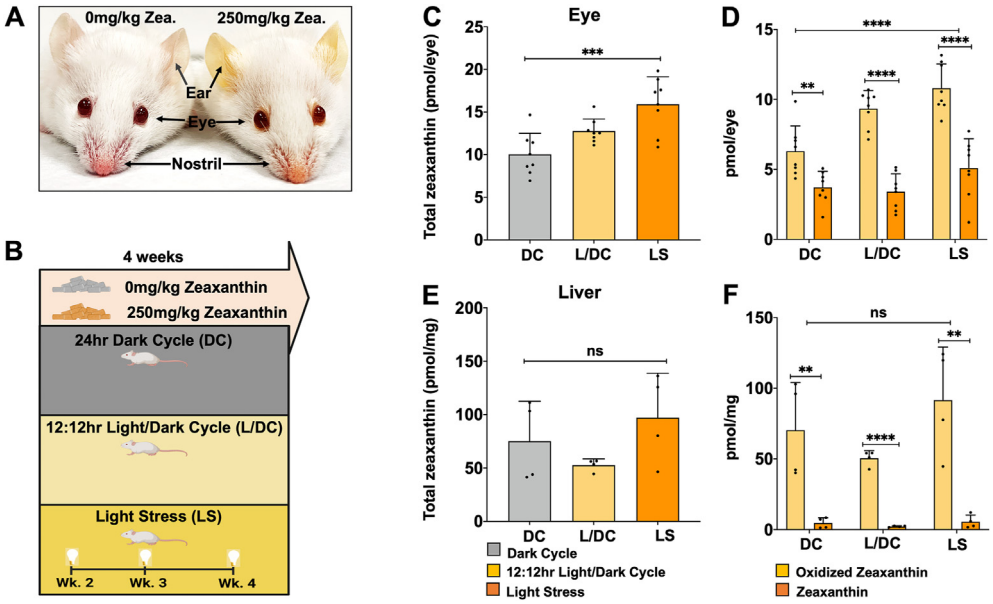

Figure 7: Light affects ocular zeaxanthin metabolism of albino *Isx*$^{-/-}$/*Bco2*$^{-/-}$ mice. *Isx*$^{-/-}$/*Bco2*$^{-/-}$ mice with a C57/BL6 genetic background were crossed with B6(Cg)-Tyrc−2J/J mice to produce mice displaying an albino phenotype. Mice were raised on either 0 mg/kg zeaxanthin as the non-supplemental control diet or 250 mg/kg zeaxanthin diet for 4 weeks. **A)** Photograph of albino *Isx*$^{-/-}$/*Bco2*$^{-/-}$ mice on 0 mg/kg zeaxanthin (left) or 250 mg/kg zeaxanthin (right) diet. The yellow skin phenotype was observed in the ears, eyelids, and nostrils of *Isx*$^{-/-}$/*Bco2*$^{-/-}$ mice on a 250 mg/kg zeaxanthin diet. **B)** Schematic of the experimental design of the light stress study. 4-week-old albino *Isx*$^{-/-}$/*Bco2*$^{-/-}$ mice were supplemented with a 250 mg/kg 3R,3′R-zeaxanthin diet or control diet for 4 weeks. During the 4 weeks of dietary intervention, mice were separated into one of the three experimental groups. These included 24 h dark cycle group (DC), a normal 12hr light−dark cycle group (L/DC), and a light stress group (LC) that received a light insult biweekly for 2 min at 85,000 lux. **C)** Total zeaxanthin from the whole eye from *Isx*$^{-/-}$/*Bco2*$^{-/-}$ mice under different light conditions. **D)** Ocular concentration of oxidized and parent zeaxanthin isolated from eyes of *Isx*$^{-/-}$/*Bco2*$^{-/-}$ mice under different light conditions. **E)** Total hepatic zeaxanthin concentration from the liver of *Isx*$^{-/-}$/*Bco2*$^{-/-}$ mice under different light conditions. **F)** Oxidized and parent zeaxanthin isolated from the liver of *Isx*$^{-/-}$/*Bco2*$^{-/-}$ mice in different light conditions. Values indicate means ± SD from four (2 females and 2 males) mice. Statistical analyses were performed by comparing tissues using two-way ANOVA. $^{*}P < 0.05$; $^{**}P < 0.005$, $^{***}P < 0.0001$. Statistical significance for oxidized and parent zeaxanthin between different dietary groups was analyzed using an unpaired two-tailed Student's *t*-test. $^{*}P < 0.05$, $^{**}P < 0.01$, $^{***}P < 0.001$, $^{****}P < 0.001$. Statistical significance was determined using Prism 8 software, with a significance threshold set at $P < 0.05$.

Studies from our and other laboratories revealed that SR-B1 plays a critical role in the uptake of carotenoids and fat-soluble vitamins in enterocytes [34,45]. For instance, we previously showed that knockout of the SR-B1 gene impedes xanthophyll absorption in the mouse intestine [35]. Other studies demonstrated that the vitamin A status of the host influences the absorption of carotenoids. The molecular equivalent for this regulation is the transcription factor ISX that controls intestinal expression of BCO1 and SR-B1 in enterocytes of the intestine [30,37,46]. Therefore, we established an *Isx*$^{-/-}$/*Bco2*$^{-/-}$ double mutant mouse and compared it with the respective single *Bco2*$^{-/-}$ mutant mice. The double-knockout mice displayed significantly higher concentrations of zeaxanthin metabolites than the single-knockout mice in different parts of the small intestine, liver, and peripheral tissues. In the small intestine, the highest concentration of carotenoids was detected in the jejunum. The enhanced accumulation of carotenoids in double mutant mice was observed on diets that provided physiological and supra-physiological concentrations of zeaxanthin. We found the following evidence that the differences between genotypes were mainly caused by alterations in intestinal absorption of the pigments. First, intestinal SR-B1 expression was higher in the double than in the single knockout mice and WT mice in all parts of the intestine. Second, we demonstrated by comparing the carotenoid content in feces that the double knockout excreted less carotenoids than the single knockout under low and high supplementation conditions, indicating that they absorbed more zeaxanthin. Notably, zeaxanthin diets were prepared without vitamin A supplement and we expected that the absence of vitamin A should affect the ISX-SR-B1 axis and increase the intestinal activity of SR-B1. In fact, zeaxanthin concentration in the fecal matter of *Bco2*$^{-/-}$ mice slowly decreased during the intervention and approached the levels of *Isx*$^{-/-}$/*Bco2*$^{-/-}$ mice. This finding suggested that the effect of dietary vitamin A deprivation on intestinal ISX expression was established slowly over time. However, the enhanced accumulation of zeaxanthin and its metabolites in *Isx*$^{-/-}$/*Bco2*$^{-/-}$ mice suggested that the *Isx* genotype affected additional components of intestinal lipid absorption. Indeed, we recently observed that ISX affects lipoprotein metabolism and chylomicron kinetics in mice supplemented with β-carotene [47]. Future studies are needed to fully elucidate the role of ISX in lipid metabolism.

We also observed that zeaxanthin is rapidly oxidized to a less polar metabolite in mouse tissues. We established chiral chromatography in combination with mass spectrometry to identify the oxidized metabolites as ε,ε-carotene-3,3′-diones. This keto-carotenoid displayed chiral centers at C6 and C6′ and we detected all three enantiomers though they existed in different concentrations. Additionally, we detected parent zeaxanthin (3R, 3′R-β,β-carotene-diol) in tissues and putative *cis*-derivatives. Recently, an enzyme, BDH1L catalyzing such oxidation of dietary xanthophyll was identified in birds and fish [48]. Mammalian genomes encode related dehydrogenases but not a BDH1L homolog. The existence of different stereoisomers indicated that the oxidation of the 3-hydroxy-group to the corresponding 3-oxo-group and the rearrangement of the double bonds is not catalyzed in a stereospecific manner in mice. For birds and fish the isomeric composition of ε,ε-carotene-3,3′-diones has not been determined to our best knowledge. It will be worthwhile to study in the future whether

the production of ε,ε-carotene-3,3′-dione in mammals, birds, and fish is catalyzed by similar or different mechanisms.

Another interesting finding was that the ratio between zeaxanthin and ε,ε-carotene-3,3′-diones differed between tissues and was seemingly affected by the supplementation regimen. This variation indicates that tissues display specific metabolic profiles for dietary zeaxanthin. For instance, the subcellular distribution of the pigments and compartmentalized enzyme activities may contribute to these tissue profiles. Recently, members of the ASTER protein family have been demonstrated to mediate non-vesicular transport of carotenoids between cellular membranes and expose them to metabolizing enzymes [15,49,50].

The advanced understating of factors that determine carotenoid absorption and tissue levels as presented here, allowed us to generate an albino *Isx*$^{-/-}$/*Bco2*$^{-/-}$ mouse model. These knockout mice display a C57/b6 genetic background. This novel mouse strain is a resourceful animal model to characterize the physiological roles and benefits of various carotenoids. The lack of melanin pigmentation will allow for the studying of the photo-protective role of carotenoid pigments in the skin and eyes. Notably, these mice rapidly accumulated carotenoids in the skin and displayed hypercarotenemia. This characteristic may allow studying the role of carotenoids in dermal protection from UV irradiation and other skin irritants in future studies. We have already begun studying ocular carotenoid metabolism in this mouse model. A standard repertoire of morphometric and functional measures, including OCT and ERG, revealed that zeaxanthin accumulation did not affect the retina of these mice in a negative fashion. This is consistent with studies in pigmented *Bco2*$^{-/-}$ mice [51,52]. We here added an additional mechanism that may contribute to the eye-protective effects of zeaxanthin. For this purpose, we subjected the albino mouse line to different light regimens. Interestingly, we observed that carotenoid concentration increased light-dependently in the eyes. More importantly, there was a significant effect of light on the composition of zeaxanthin metabolites. Dark-raised mice displayed the lowest ratio between parent and oxidized zeaxanthin. In light-reared mice, the ratio increased in favor of the oxidized form that existed in different stereoisomers. In mice subjected to light stress, the ratio further increased in favor of ε,ε-carotene-3,3′-dione stereoisomers. Zeaxanthin is the major macula pigment in the primate [3] and oxidation of macula pigments to keto-carotenoids have been observed in the human retina and blood [53,54]. The light-dependent increase of oxidized zeaxanthin metabolites in the mouse eyes demonstrates the capacity of ocular tissues to catalyze the complex chemical transformation of carotenoids and suggests that carotenoids may act as redox-active compounds under light stress. It is noteworthy that the formation of lutein enantiomers has been also described in the primate eyes as well and is associated with *meso*-zeaxanthin accumulation [4]. It will be fascinating to study whether lutein is processed similarly in the albino *Isx*$^{-/-}$/*Bco2*$^{-/-}$ mouse as described in humans.

Taken together, we here studied factors that determine carotenoid accumulation in mice. A major finding was that expression of BCO2 in the gut serves as a gatekeeper of this process. We propose that high expression of BCO2 in mice prevents carotenoid accumulation, whereas low expression of BCO2 favors this process in humans and other vertebrates. As an additional host factor, the absorption of carotenoids is significantly influenced by the ISX/SR-B1 axis. This finding confirms genetic studies at the biochemical level, suggesting that SR-BI and ISX are major factors that influence carotenoid absorption and body distribution in humans [45]. The genetic manipulation of mice led to phenotypes previously described in humans such as hypercarotenemia. Furthermore, when zeaxanthin is absorbed in mice, chemical modifications of its ionone rings take place and this modification is influenced by tissue factors and light. In the future, the albino *Isx*$^{-/-}$/*Bco2*$^{-/-}$ mouse model will be a resourceful model to study carotenoid functions in health and disease. A better understanding of the pigments' beneficial and putative detrimental effects will allow science-based recommendations for the intake of these essential nutrients.

FUNDING SOURCES

This work was supported by the National Eye Institute (EY020551 and EY028121), the T32 Visual Science Training Grant (EY007157), and the P30 Visual Science Core Grant (EY011373).

DECLARATION OF COMPETING INTEREST

None declared.

DATA AVAILABILITY

Data will be made available on request.

ACKNOWLEDGMENTS

We thank all the members of our laboratory for their valuable suggestions and the visual science core (EY011373) of Case Western Reserve University for their expert support.

APPENDIX A. SUPPLEMENTARY DATA

Supplementary data to this article can be found online at https://doi.org/10.1016/j.molmet.2023.101742.

REFERENCES

[1] Eggersdorfer M, Wyss A. Carotenoids in human nutrition and health. Arch Biochem Biophys 2018;652:18—26.
[2] Snodderly DM, Handelman GJ, Adler AJ. Distribution of individual macular pigment carotenoids in central retina of macaque and squirrel monkeys. Invest Ophthalmol Vis Sci 1991;32(2):268—79.
[3] Li B, George EW, Rognon GT, Gorusupudi A, Ranganathan A, Chang FY, et al. Imaging lutein and zeaxanthin in the human retina with confocal resonance Raman microscopy. Proc Natl Acad Sci U S A 2020;117(22):12352—8.
[4] Bernstein PS, Li B, Vachali PP, Gorusupudi A, Shyam R, Henriksen BS, et al. Lutein, zeaxanthin, and meso-zeaxanthin: the basic and clinical science underlying carotenoid-based nutritional interventions against ocular disease. Prog Retin Eye Res 2016;50:34—66.
[5] Mares J. Lutein and zeaxanthin isomers in eye health and disease. Annu Rev Nutr 2016;36:571—602.
[6] Grune T, Lietz G, Palou A, Ross AC, Stahl W, Tang G, et al. Beta-carotene is an important vitamin A source for humans. J Nutr 2010;140(12):2268S—85S.
[7] von Lintig J, Moon J, Babino D. Molecular components affecting ocular carotenoid and retinoid homeostasis. Prog Retin Eye Res 2021;80:100864.
[8] Bohn T, Bonet ML, Borel P, Keijer J, Landrier JF, Milisav I, et al. Mechanistic aspects of carotenoid health benefits - where are we now? Nutr Res Rev 2021;34(2):276—302.
[9] Miller AP, Coronel J, Amengual J. The role of beta-carotene and vitamin A in atherogenesis: evidences from preclinical and clinical studies. Biochim Biophys Acta Mol Cell Biol Lipids 2020:158635.

[10] Johnson EJ. Role of lutein and zeaxanthin in visual and cognitive function throughout the lifespan. Nutr Rev 2014;72(9):605–12.
[11] Chew EY, SanGiovanni JP, Ferris FL, Wong WT, Agron E, Clemons TE, et al. Lutein/zeaxanthin for the treatment of age-related cataract: AREDS2 randomized trial report no. 4. JAMA Ophthalmol 2013;131(7):843–50.
[12] Goodman GE, Thornquist MD, Balmes J, Cullen MR, Meyskens Jr FL, Omenn GS, et al. The Beta-Carotene and Retinol Efficacy Trial: incidence of lung cancer and cardiovascular disease mortality during 6-year follow-up after stopping beta-carotene and retinol supplements. J Natl Cancer Inst 2004;96(23):1743–50.
[13] Omenn GS, Goodman GE, Thornquist MD, Balmes J, Cullen MR, Glass A, et al. Effects of a combination of beta carotene and vitamin A on lung cancer and cardiovascular disease. N Engl J Med 1996;334(18):1150–5.
[14] Bohn T, Desmarchelier C, Dragsted LO, Nielsen CS, Stahl W, Ruhl R, et al. Host-related factors explaining interindividual variability of carotenoid bioavailability and tissue concentrations in humans. Mol Nutr Food Res 2017;61(6).
[15] Bandara S, von Lintig J. Aster la vista: unraveling the biochemical basis of carotenoid homeostasis in the human retina. Bioessays 2022;44(11): e2200133.
[16] Voolstra O, Kiefer C, Hoehne M, Welsch R, Vogt K, von Lintig J. The Drosophila class B scavenger receptor NinaD-I is a cell surface receptor mediating carotenoid transport for visual chromophore synthesis. Biochemistry 2006;45(45):13429–37.
[17] Kiefer C, Sumser E, Wernet MF, Von Lintig J. A class B scavenger receptor mediates the cellular uptake of carotenoids in Drosophila. Proc Natl Acad Sci USA 2002;99(16):10581–6.
[18] Borel P, Lietz G, Goncalves A, Szabo de Edelenyi F, Lecompte S, Curtis P, et al. CD36 and SR-BI are involved in cellular uptake of provitamin A carotenoids by Caco-2 and HEK cells, and some of their genetic variants are associated with plasma concentrations of these micronutrients in humans. J Nutr 2013;143(4): 448–56.
[19] During A, Doraiswamy S, Harrison EH. Xanthophylls are preferentially taken up compared with beta-carotene by retinal cells via a SRBI-dependent mechanism. J Lipid Res 2008;49(8):1715–24.
[20] Vage DI, Boman IA. A nonsense mutation in the beta-carotene oxygenase 2 (BCO2) gene is tightly associated with accumulation of carotenoids in adipose tissue in sheep (Ovis aries). BMC Genet 2010;11:10.
[21] Tian R, Pitchford WS, Morris CA, Cullen NG, Bottema CD. Genetic variation in the beta, beta-carotene-9', 10'-dioxygenase gene and association with fat colour in bovine adipose tissue and milk. Anim Genet 2009;41:253–9.
[22] Strychalski J, Brym P, Czarnik U, Gugolek A. A novel AAT-deletion mutation in the coding sequence of the BCO2 gene in yellow-fat rabbits. J Appl Genet 2015;56(4):535–7.
[23] Eriksson J, Larson G, Gunnarsson U, Bed'hom B, Tixier-Boichard M, Stromstedt L, et al. Identification of the yellow skin gene reveals a hybrid origin of the domestic chicken. PLoS Genet 2008;4(2):e1000010.
[24] Bandara S, Thomas LD, Ramkumar S, Khadka N, Kiser PD, Golczak M, et al. The structural and biochemical basis of apocarotenoid processing by beta-carotene oxygenase-2. ACS Chem Biol 2021;16(3):480–90.
[25] Kelly ME, Ramkumar S, Sun W, Colon Ortiz C, Kiser PD, Golczak M, et al. The biochemical basis of vitamin A production from the asymmetric carotenoid beta-cryptoxanthin. ACS Chem Biol 2018;13(8):2121–9.
[26] Toomey MB, Lopes RJ, Araujo PM, Johnson JD, Gazda MA, Afonso S, et al. High-density lipoprotein receptor SCARB1 is required for carotenoid coloration in birds. Proc Natl Acad Sci U S A 2017;114(20):5219–24.
[27] Meyers KJ, Johnson EJ, Bernstein PS, Iyengar SK, Engelman CD, Karki CK, et al. Genetic determinants of macular pigments in women of the carotenoids in age-related eye disease study. Invest Ophthalmol Vis Sci 2013;54(3):2333–45.
[28] Sy C, Gleize B, Dangles O, Landrier JF, Veyrat CC, Borel P. Effects of physicochemical properties of carotenoids on their bioaccessibility, intestinal cell uptake, and blood and tissue concentrations. Mol Nutr Food Res 2012;56(9): 1385–97.
[29] Amengual J, Lobo GP, Golczak M, Li HN, Klimova T, Hoppel CL, et al. A mitochondrial enzyme degrades carotenoids and protects against oxidative stress. Faseb J 2011;25(3):948–59.
[30] Choi MY, Romer AI, Hu M, Lepourcelet M, Mechoor A, Yesilaltay A, et al. A dynamic expression survey identifies transcription factors relevant in mouse digestive tract development. Development 2006;133(20):4119–29.
[31] Thomas LD, Bandara S, Parmar VM, Srinivasagan R, Khadka N, Golczak M, et al. The human mitochondrial enzyme BCO2 exhibits catalytic activity toward carotenoids and apocarotenoids. J Biol Chem 2020;295(46):15553–65.
[32] Ramkumar S, Parmar VM, Samuels I, Berger NA, Jastrzebska B, von Lintig J. The vitamin A transporter STRA6 adjusts the stoichiometry of chromophore and opsins in visual pigment synthesis and recycling. Hum Mol Genet 2022;31(4):548–60.
[33] Moon J, Ramkumar S, von Lintig J. Genetic dissection in mice reveals a dynamic crosstalk between the delivery pathways of vitamin A. J Lipid Res 2022;63(6):100215.
[34] von Lintig J, Moon J, Lee J, Ramkumar S. Carotenoid metabolism at the intestinal barrier. Biochim Biophys Acta Mol Cell Biol Lipids 2020;1865(11): 158580.
[35] Widjaja-Adhi MA, Lobo GP, Golczak M, Von Lintig J. A genetic dissection of intestinal fat-soluble vitamin and carotenoid absorption. Hum Mol Genet 2015;24(11):3206–19.
[36] Widjaja-Adhi MAK, Palczewski G, Dale K, Knauss EA, Kelly ME, Golczak M, et al. Transcription factor ISX mediates the cross talk between diet and immunity. Proc Natl Acad Sci U S A 2017;114(43):11530–5.
[37] Seino Y, Miki T, Kiyonari H, Abe T, Fujimoto W, Kimura K, et al. Isx participates in the maintenance of vitamin A metabolism by regulation of beta-carotene 15,15'-monooxygenase (Bcmo1) expression. J Biol Chem 2008;283(8):4905–11.
[38] Nagao A, Maoka T, Ono H, Kotake-Nara E, Kobayashi M, Tomita M. A 3-hydroxy beta-end group in xanthophylls is preferentially oxidized to a 3-oxo epsilon-end group in mammals. J Lipid Res 2015;56(2):449–62.
[39] Granado-Lorencio F, Blanco-Navarro I, Perez-Sacristan B, Hernandez-Alvarez E. Biomarkers of carotenoid bioavailability. Food Res Int 2017;99(Pt 2): 902–16.
[40] Lee CM, Boileau AC, Boileau TW, Williams AW, Swanson KS, Heintz KA, et al. Review of animal models in carotenoid research. J Nutr 1999;129(12):2271–7.
[41] Raghuvanshi S, Reed V, Blaner WS, Harrison EH. Cellular localization of beta-carotene 15,15' oxygenase-1 (BCO1) and beta-carotene 9',10' oxygenase-2 (BCO2) in rat liver and intestine. Arch Biochem Biophys 2015;572:19–27.
[42] Toews DPL, Hofmeister NR, Taylor SA. The evolution and genetics of carotenoid processing in animals. Trends Genet 2017;33(3):171–82.
[43] Kiefer C, Hessel S, Lampert JM, Vogt K, Lederer MO, Breithaupt DE, et al. Identification and characterization of a mammalian enzyme catalyzing the asymmetric oxidative cleavage of provitamin A. J Biol Chem 2001;276(17): 14110–6.
[44] Lindqvist A, He YG, Andersson S. Cell type-specific expression of beta-carotene 9',10'-monooxygenase in human tissues. J Histochem Cytochem 2005;53(11):1403–12.
[45] Borel P, Desmarchelier C. Bioavailability of fat-soluble vitamins and phytochemicals in humans: effects of genetic variation. Annu Rev Nutr 2018;38: 69–96.
[46] Lobo GP, Hessel S, Eichinger A, Noy N, Moise AR, Wyss A, et al. ISX is a retinoic acid-sensitive gatekeeper that controls intestinal beta,beta-carotene absorption and vitamin A production. Faseb J 2010;24(6):1656–66.

[47] Moon J, Ramkumar S, von Lintig J. Genetic tuning of beta-carotene oxygenase-1 activity rescues cone photoreceptor function in STRA6-deficient mice. Hum Mol Genet 2023;32(5):789–809.

[48] Toomey MB, Marques CI, Araujo PM, Huang D, Zhong S, Liu Y, et al. A mechanism for red coloration in vertebrates. Curr Biol 2022;32(19):4201–4214 e4212.

[49] Bandara S, Ramkumar S, Imanishi S, Thomas LD, Sawant OB, Imanishi Y, et al. Aster proteins mediate carotenoid transport in mammalian cells. Proc Natl Acad Sci U S A 2022;119(15):e2200068119.

[50] Bandara S, Moon J, Ramkumar S, von Lintig J. ASTER-B regulates mitochondrial carotenoid transport and homeostasis. J Lipid Res 2023:100369.

[51] Li B, Rognon GT, Mattinson T, Vachali PP, Gorusupudi A, Chang FY, et al. Supplementation with macular carotenoids improves visual performance of transgenic mice. Arch Biochem Biophys 2018;649:22–8.

[52] Widjaja-Adhi MAK, Ramkumar S, von Lintig J. Protective role of carotenoids in the visual cycle. Faseb J 2018:fj201800467R.

[53] Khachik F, Bernstein PS, Garland DL. Identification of lutein and zeaxanthin oxidation products in human and monkey retinas. Invest Ophthalmol Vis Sci 1997;38(9):1802–11.

[54] Khachik F, de Moura FF, Zhao DY, Aebischer CP, Bernstein PS. Transformations of selected carotenoids in plasma, liver, and ocular tissues of humans and in nonprimate animal models. Invest Ophthalmol Vis Sci 2002;43(11):3383–92.

